J Mater Sci (2011) 46:4588–4597
DOI 10.1007/s10853-011-5358-2

Enhanced compressive response of hybrid Mg–CNT nano-composites

M. K. Habibi · M. Paramsothy · A. M. S. Hamouda · M. Gupta

Received: 23 December 2010 / Accepted: 31 January 2011 / Published online: 11 February 2011

Abstract Uniaxial compressive properties of hybrid Mg/Al–CNT nano-composites are studied in the present paper. Hybrid nano-composites were fabricated using powder metallurgy route followed by microwave assisted rapid sintering technique and hot extrusion. The hybrid Mg/Al–CNT nano-composites exhibited slightly smaller grain sizes compared to monolithic Mg and reasonable hybrid Al–CNT nano-particle distribution up to Al content of 1.00 wt%. Compared to pure Mg, the Mg/Al–CNT nano-composites exhibited higher compressive yield strength (0.2% CYS), ultimate compressive strength (UCS) and work of fracture (WOF) (up to +36%, +76%, +36%) compared to pure Mg but failure strain was compromised. Inclusive of crystallographic texture changes, the effect of hybrid Al–CNT nano-particle integration on the enhancement of compressive properties of Mg is investigated in this paper.

Introduction

Light weight materials are gaining the attention of researchers worldwide due to their ability to cut down on energy consumption and greenhouse gas emission in a number of engineering sectors. Among the light metallic structural materials, magnesium and aluminum have been commonly used. Mg is about 35% lighter than Al but both have similar melting points and strengths. However, Mg has the disadvantage of limited ductility attributed to its HCP structure while Al is more ductile due to its FCC structure. Moreover, Mg has a lower elastic modulus (40–45 GPa) than Al (69.9 GPa) [1]. Until recently, many efforts have been made to increase strength and ductility of Mg by reinforcing with metallic or ceramic particles of different sizes [2–7]. However, among the desired reinforcements, the carbon nanotube (CNT) has attracted researchers more due to its extraordinary strength (up to 150 GPa) and young's modulus (up to 1 TPa), which makes it an ideal candidate as reinforcement for high strength, light weight, and high performance composites [8–10]. It is a fact that the CNT has high aspect ratio, which makes it possible to acquire smaller interparticle spacing in the matrix at very low concentrations compared to traditional reinforcements such as SiC [11]. Therefore, the CNT can act as a more effective obstacle to dislocation movement in metals. Moreover, in the case of obstacles with high aspect ratio, dislocations cannot easily climb to circumvent the obstacle, so the expectation is not only improvement of flow stress and toughness but also a considerable improvement in creep resistance [12]. However, due to weak bonding between pure Mg and C, the synthesized composite reinforced with CNT may not be strong enough. Thus, an alternative method for using CNT as reinforcement with enhanced interfacial strength is needed. It is expected that using CNT as a constituent of a hybrid reinforcement may be a good procedure to take advantage of CNT as a reinforcement. Considering the favorable response of Mg toward Al, it can be expected that the presence of CNT as a constituent of hybrid Al–CNT nano-particles may further enhance the mechanical response of magnesium. Results of literature search indicate that no attempt has been made to integrate magnesium with

M. K. Habibi · M. Paramsothy · M. Gupta (✉)
Department of Mechanical Engineering, National University of Singapore, 9 Engineering Drive 1, Singapore 117576, Singapore
e-mail: mpegm@nus.edu.sg

A. M. S. Hamouda
Mechanical and Industrial Engineering Department, Qatar University, P.O. Box No. 2713, Doha, Qatar

hybridized Al–CNT nano-particles for the purpose of studying the compressive behavior of the resultant nano-composites. In this work, Mg/Al–CNT nano-composites are developed where monolithic Mg is the matrix that is reinforced with hybrid particles comprised of pure Al and embedded CNTs (Fig. 1). The hybrid Mg/Al–CNT nano-composites are obtained by adding a small weight percent of ball-milled hybrid Al–CNT particles to Mg particles using the powder metallurgy route followed by microwave assisted rapid sintering technique and hot extrusion.

In recent years, researchers established that the flow stress behavior of Mg and Mg alloys in compression differs markedly from that seen in tension. In tension, deformation mechanisms by slip typically dominated whereas in compression, twinning induced deformation mechanisms dominated in Mg and Mg alloys [13–15].

Generally, the dominant deformation mechanism in Mg is basal slip, secondary (prismatic and pyramidal) slip, and $\{1\ 0\ -1\ 2\}$ tension twining and $\{1\ 0\ -1\ 1\}$ compression twinning [16, 17]. According to the recorded data, the CRSS of a basal slip system at room temperature is approximately 1/100 that of non-basal slip systems on the prismatic and pyramidal planes [16, 17]. Therefore, plastic deformation in polycrystalline Mg has been thought to occur almost entirely by basal slip. However, during compression, twinning is also mainly responsible for the material deformation. It is known that extrusion usually leads to pronounced texture with the basal plane parallel to the extrusion direction and therefore, it was expected that the tendency for twinning would be increased during compression with a consequent increase in tension/compression anisotropy in yield strength [18]. Twinning modes in hcp metals are distinguished by their ability to produce either tensile or compressive strain along the crystallographic *c*-axis, but not both. Depending upon the *c*/*a* axial ratio, hcp twinning's mode may be either tensile or compressive. In the case of magnesium, the twinning dominant mode $\{1\ 0\ -1\ 2\}\ \langle 1\ 0\ -1\ 1\rangle$ is a tensile twin since $c/a = 1.624$ (less than 1.732) [14, 19]. It seems that during compression of magnesium based material, tension twinning and then basal and finally non-basal slips (in that order) are responsible for the deformation, respectively [14].

Accordingly, this study discusses the effect of hybrid Al–CNT particles on the enhancement in compressive strength of Mg/Al–CNT nano-composites compared to pure Mg. An investigation is also made on the evolution of crystallographic texture due to addition of hybrid Al–CNT particles as well as applying compressive deformation.

Experimental procedures

Materials

In this study, magnesium powder (98.5% purity, 60–300 μm particles size range) supplied by Merck (Germany) was used as the matrix material. Carbon nanotubes (vapor grown, 94.7% purity, 40–70 nm OD) supplied by Nanostructured & Amorphous Materials Inc (Texas, USA) and aluminum powder (7–15 μm particle size) supplied by Alfa Aesar (USA) were used as the reinforcement.

Processing

Preparation of composite reinforcements

In order to prepare different reinforcement for different nano-composite formulations, the content of CNT particles was kept constant at 0.18 wt% [20] while that of Al particles was varied. 0.30 wt% stearic acid was used as the process control agent (PCA). In the first stage, Al and CNT particles were blended with stearic acid for 1 h using RETSCH PM-400 mechanical alloying machine. In the

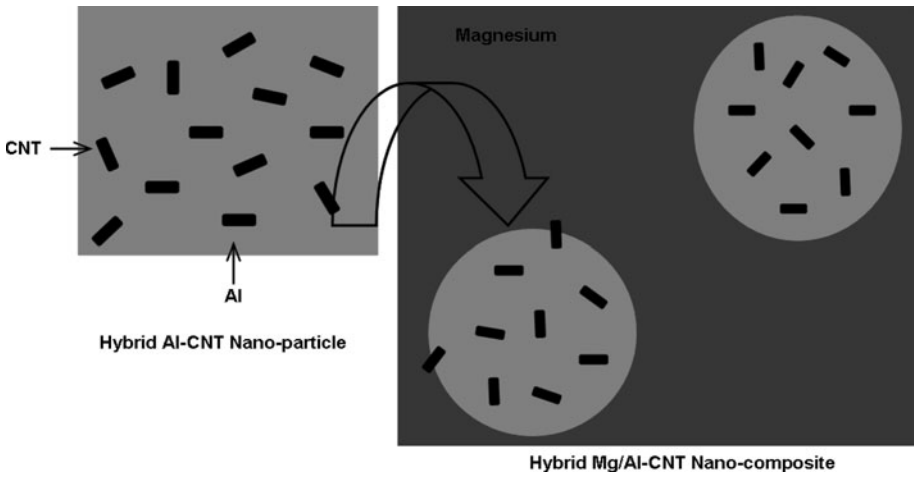

Fig. 1 Schematic of hybrid Mg/Al–CNT nano-composite synthesized in this work

second stage, steel balls were added and the blended mixture was ball-milled for 2 h. Ball to powder ratio was kept at 20:1 and the ball milling speed was set at 200 rpm during both blending and ball milling steps. For the preparation of Mg matrix nano-composites, no steel balls were used during blending as explained in the next section.

Primary processing

The magnesium matrix nano-composites were synthesized using the powder metallurgy technique. The synthesis process involved blending pure magnesium powder with the hybrid Al–CNT nano-particles in a RETSCH PM-400 mechanical alloying machine at 200 rpm for 60 min. The blended powder mixture was compacted at a pressure of 97 bar (load: 50 tons) to compacts (40-mm height, 35-mm diameter) using a 100-ton press. All compacts (inclusive of pure Mg compact) were sintered using hybrid microwave assisted 2-directional sintering technique. The compacts were heated for 13 min to a temperature near the melting point of magnesium in a 900 W, 2.45 GHz SHARP microwave oven using colloidal graphite as an oxidation barrier layer.

Secondary processing

All sintered compacts were hot extruded at a temperature of 350 °C with an extrusion ratio of 26:1 using a 150-ton hydraulic press. Before extrusion, the compacts were coated with colloidal graphite and soaked at 400 °C for 1 h. Final diameter of the rods obtained after the extrusion was 7 mm.

Microstructural characterization

Microstructural characterization studies were conducted on metallographically polished extruded samples to investigate morphological characteristics of grains and reinforcement distribution. Hitachi FESEM-S4300 field emission scanning electron microscope equipped with energy dispersive X-ray spectroscopy (EDS), Olympus metallographic optical microscope and Scion image analysis software were used for this purpose. Crystallographic texture measurements were carried out on samples of monolithic Mg and its hybrid Mg/Al–CNT nano-composite formulations to determine the dominant textures in the transverse and longitudinal (extrusion) directions. The measurements were made with a Shimadzu LAB-X XRD-6000 diffractometer. The samples were exposed to Cu Kα radiation ($\lambda = 1.054056$ Å). The texture was measured in the as-extruded condition (before compression) as well as after prescribed compressive deformation.

Hardness

Microhardness measurements were made on the polished samples of extruded monolithic Mg and hybrid Mg/Al–CNT nano-composite rods using a Shimadzu HMV 50 automatic digital microhardness tester. The microhardness tests were performed using a Vickers indenter under a test load of 25 gf and a dwell time of 15 s in accordance with the ASTM standard E3 84-99.

Compressive testing

Room temperature compressive tests were performed on cylindrical monolithic and hybrid nano-composite samples according to ASTM E9-89a using an automated servo hydraulic testing machine (MTS 810) with a crosshead speed set at 0.04 mm/min. Extruded rod of 7 mm diameter was cut into 7 mm length samples for compression tests to provide the aspect ratio (l/d) of 1.0. The compression load was applied parallel to the extrusion direction. Teflon tape was placed between the contacting surfaces of the specimen and machine steel platen for lubrication (to avoid barreling).

Fracture behavior

Fracture surface characterization studies were carried out on the compressive fracture surface of monolithic Mg and hybrid Mg/Al–CNT nano-composites with the objective of establishing the failure mechanism. Fractography was accomplished using a FESEM-S4300.

Results

Microstructural characteristics

Microstructural characterization studies conducted on Mg/Al–CNT nano-composite samples indicated reasonably uniform distribution of the hybrid Al–CNT nano-particles in the Mg matrix up to Al content of 1.00 wt%. Reinforcement clustering occurred with further increase in Al content of hybrid Al–CNT nano-particles (Fig. 2a–c). Due to very low content of CNT (0.18 wt%), CNTs could not be detected easily within the hybrid Al–CNT nano-particles [21].

As listed in Table 1, the average grain size in the case of Mg/Al–CNT nano-composites was significantly smaller compared to monolithic Mg suggesting the ability of hybrid Al–CNT nano-particles to serve either as nucleation sites or obstacles to grain growth during processing.

Texture results are listed in Table 2 and shown in Fig. 3. The dominant texture in transverse and longitudinal

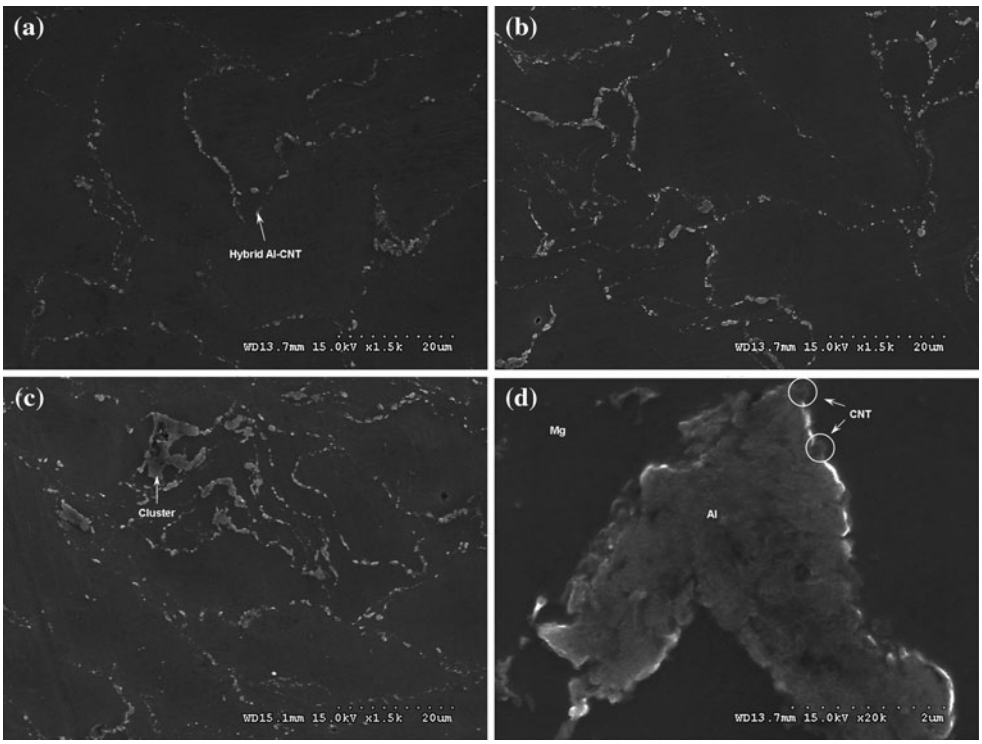

Fig. 2 Representive micrographs showing distribution of hybrid Al–CNT nano-particles through the matrix in: **a** Mg/0.50Al–0.18CNT, **b** Mg/1.00Al–0.18CNT, **c** Mg/1.50Al–0.18CNT, and **d** high magnification of a hybrid Al–CNT cluster

Table 1 Results of grain morphology

Material	Reinforcement (wt%)		Grain size (μm)	Aspect ratio
	Al	CNT		
Mg	–	–	19 ± 4	1.5 ± 0.3
Mg/0.50Al–0.18CNT	0.50	0.18	10 ± 3	1.7 ± 0.5
Mg/1.00Al–0.18CNT	1.00	0.18	8 ± 3	1.7 ± 0.4
Mg/1.50Al–0.18CNT	1.50	0.18	8 ± 4	1.8 ± 0.5

directions in the case of monolithic Mg was (1 0 −1 1). However, in the case of hybrid Mg/Al–CNT nano-composites, the dominant textures in the transverse and longitudinal directions were (1 0 −1 0) and (0 0 0 2), respectively. It seems that presence of hybrid Al–CNT nano-particles caused basal plane reorientation parallel to the extrusion direction. The crystallographic texture significantly changed after compressive deformation mostly due to activation of tensile twinning during compression in monolithic Mg and all hybrid Mg/Al–CNT nano-composites. The dominant texture in transverse and longitudinal direction of compressively deformed monolithic Mg changed to (0 0 0 2) and (1 0 −1 1), respectively. Since the derivation of texture in a given direction involves diffraction from crystallographic planes parallel or near-parallel (±20°) [22, 23] to the plane containing the direction vector, the schematic representation of dominant texture in Fig. 3b for monolithic Mg is considered appropriate. However, in the case of hybrid Mg/Al–CNT nano-composites, the dominant textures in the transverse and longitudinal direction were (1 0 −1 0) and (0 0 0 2), respectively.

Hardness

Results of microhardness measurements are given in Table 3. Hybrid Mg/Al–CNT nano-composites exhibited significantly higher hardness compared to monolithic Mg. The average microhardness in the case of nano-composites increased with increase in Al content of hybrid Al–CNT nano-particles.

Stress–strain curves

The compressive stress–strain curves for pure Mg and hybrid Mg/Al–CNT nano-composites are shown in Fig. 4.

Table 2 Texture results of Mg and Mg/Al–CNT nano-composites based on X-ray diffraction

Material	Section	Plane	(Average I/I^{a}_{max})[b]	(Average I/I^{a}_{max})[c]
Mg	T	1 0 −1 0 prism	0.96	0.02
		0 0 0 2 basal	0.66	**1.00**
		1 0 −1 1 pyramidal	**1.00**	0.19
	L	1 0 −1 0 prism	0.23	0.56
		0 0 0 2 basal	0.63	0.77
		1 0 −1 1 pyramidal	**1.00**	**1.00**
Mg/0.50Al–0.18CNT	T	1 0 −1 0 prism	**1.00**	0.03
		0 0 0 2 basal	0.23	**1.00**
		1 0 −1 1 pyramidal	0.98	0.20
	L	1 0 −1 0 prism	0.08	**1.00**
		0 0 0 2 basal	**1.00**	0.34
		1 0 −1 1 pyramidal	0.64	0.98
Mg/1.00Al–0.18CNT	T	1 0 −1 0 prism	**1.00**	0.02
		0 0 0 2 basal	0.16	**1.00**
		1 0 −1 1 pyramidal	0.86	0.22
	L	1 0 −1 0 prism	0.06	**1.00**
		0 0 0 2 basal	**1.00**	0.23
		1 0 −1 1 pyramidal	0.44	0.17
Mg/1.50Al–0.18CNT	T	1 0 −1 0 prism	**1.00**	0.02
		0 0 0 2 basal	0.08	**1.00**
		1 0 −1 1 pyramidal	0.99	0.17
	L	1 0 −1 0 prism	0.06	**1.00**
		0 0 0 2 basal	**1.00**	0.17
		1 0 −1 1 pyramidal	0.44	0.80

T transverse, *L* longitudinal

[a] I_{max} is XRD maximum intensity from either prism, basal or pyramidal planes

[b] As-extruded condition (before compression)

[c] After compression

The bold values show the dominant texture compared to others

Curves for monolithic Mg and all hybrid Mg/Al–CNT nano-composites showed similar concave regions after yielding at point A. Beyond the concave region, more rapid work hardening rates were observed in the case of hybrid nano-composites compared to monolithic Mg (point B). In the case of monolithic Mg, work hardening steadily increased up to a peak stress followed by softening (point C) while in the case of hybrid Mg/Al–CNT nano-composites, rapid work hardening up to peak stress was followed by a sudden failure without further deformation (point D). These observations revealed that hybrid nano-composite behavior did not follow the matrix softening behavior in the last stage of deformation.

Compressive properties

The results of ambient temperature compressive tests as listed in Table 3 revealed considerable improvement in 0.2% compressive yield strength (0.2% CYS), ultimate compressive strength (UCS), and work of fracture (WOF) of hybrid Mg/Al–CNT nano-composites compared to monolithic Mg. However, failure strain was compromised. Among the nano-composite formulations, Mg/1.00Al–0.18CNT showed the best improvement in overall mechanical properties with an increase in 0.2% CYS (36%), UCS (76%), and in WOF (36%). The WOF was determined by computing the area under the stress–strain curve until the point of fracture. Figure 4 reveals the overall improvement of compressive properties in the case of Mg/Al–CNT nano-composites compared to monolithic Mg.

0.2% CYS also exhibited a near perfect linear relationship with microhardness (Hv) (Fig. 5). The relationship can be expressed as:

$$0.2\%\,\mathrm{CYS} = 1.7419\mathrm{Hv} + 34.919 \quad R^2 = 0.9466 \qquad (1)$$

Fracture behavior

Following compressive testing, monolithic samples split into two parts and fracture surfaces of all monolithic samples were inclined at an angle of 45° (45° shear failure) [24]. In comparison, hybrid nano-composite samples shattered into three parts (see Fig. 6). FESEM study of fracture surfaces revealed presence of shear bands in both monolithic and nano-composite samples (Fig. 6).

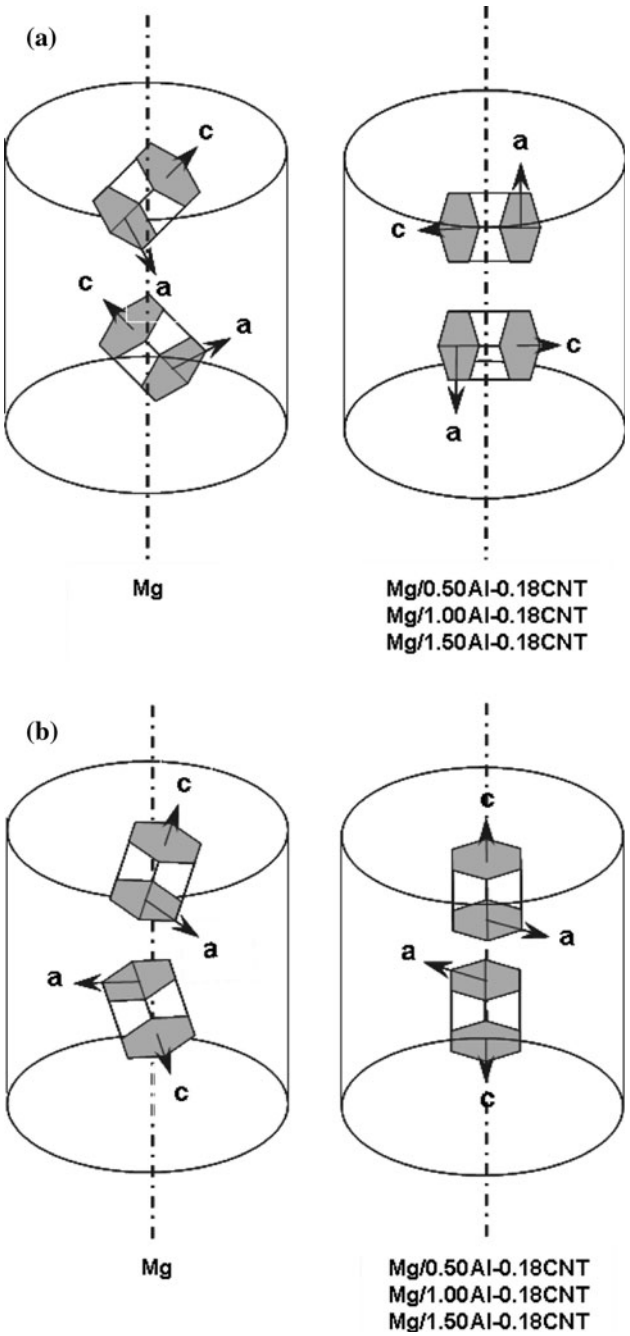

Fig. 3 Schematic diagram showing textures of monolithic Mg and Mg/Al–CNT nano-composites based on X-ray diffraction in: **a** as extruded condition and **b** after compressive deformation. In each case, *vertical axis* is parallel to extrusion direction. Each cell is made up of two HCP units having one common (0 0 0 2) basal plane

Discussion

Microstructural characteristics

The results of microstructural characterization revealed reasonable distribution of hybrid Al–CNT nano-particles up to Al content of 1.00 wt%. This reasonable distribution can be attributed to judicious selection of processing parameters and high extrusion ratio used in secondary processing. Significantly, low standard deviation in the microhardness of the monolithic and nano-composite samples also support the microstructural homogeneity realized in monolithic and nano-composite samples (see Table 3). However, further increase in Al content lead to reinforcement clustering (Fig. 2a–c). Nearly equiaxed grains were observed in monolithic and nano-composite materials as listed in Table 2. Grain sizes were reasonably smaller suggesting the ability of hybrid Al–CNT nano-particles to serve as either nucleation sites or obstacles to grain growth during processing.

Unlike monolithic Mg, Mg/Al–CNT nano-composites exhibited (1 0 −1 0) and (0 0 0 2) dominant textures in the transverse and longitudinal directions, respectively, as listed in Table 2 and shown in Fig. 3. Figure 3 also reveals the basal (0 0 0 2) plane orientation being mostly parallel to the compressive axis (*c*-axis perpendicular to compressive axis) due to extrusion. Under this basal plane orientation, twinning is the most favorable deformation mode in hexagonal materials. The most common type of twinning in magnesium base materials under this orientation is {1 0 −1 2} twinning [13, 14, 25]. Twinning caused rotation of basal planes from parallel to perpendicular to the compression axis (see Fig. 3) and the concave region in the stress–strain curves (Fig. 3) is also indicative of the onset of extensive twinning. These results are consistent with the findings of other researchers on hcp materials [26, 27].

Hardness

As evident from Table 3, the microhardness increased with hybrid Al–CNT nano-particle content. This increase in microhardness can be attributed to: (a) reasonably uniform distribution of harder Al–CNT nano-particles in the matrix [28], (b) higher constraint to localized matrix deformation during indentation due to presence of hybrid Al–CNT nano-particles [20, 29], and (c) reduced average matrix grain size [30]. The observed linear relationship can be justified by the fact that plastic flow usually takes place beneath the indenter during the microhardness test. Thus the microhardness number can be related to the average flow stress of the material in the volume subjected to plastic deformation [31].

Compressive behavior

The results of compressive properties characterization showed that the presence of hybrid Al–CNT nano-particles in Mg matrix increased both the 0.2% CYS and UCS (see Table 3; Fig. 4). Similar observations were made in the case of other composites based on Mg and Mg alloys

Table 3 Results of room temperature compressive properties

Material	Microhardness (Hv)	0.2% YS (MPa)	UCS (MPa)	Failure strain (%)	WOF[a] (MJ/m^3)
Mg	40 ± 2	106 ± 11	239 ± 15	19.8 ± 1.7	36 ± 1
Mg/0.50Al–0.18CNT	50 ± 4	120 ± 09	357 ± 13	11.0 ± 1.3	42 ± 4
Mg/1.00Al–0.18CNT	58 ± 3	132 ± 04	421 ± 15	12.5 ± 1.0	48 ± 1
Mg/1.50Al–0.18CNT	60 ± 4	144 ± 07	421 ± 11	11.3 ± 1.7	49 ± 1

[a] Determined from the engineering stress–strain curves

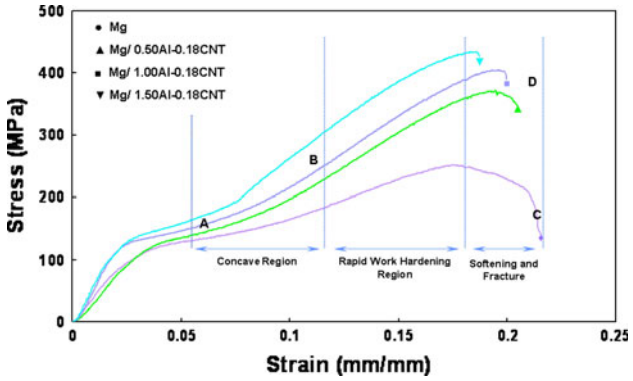

Fig. 4 Compressive stress–strain curves for monolithic Mg and hybrid Mg/Al–CNT nano-composites

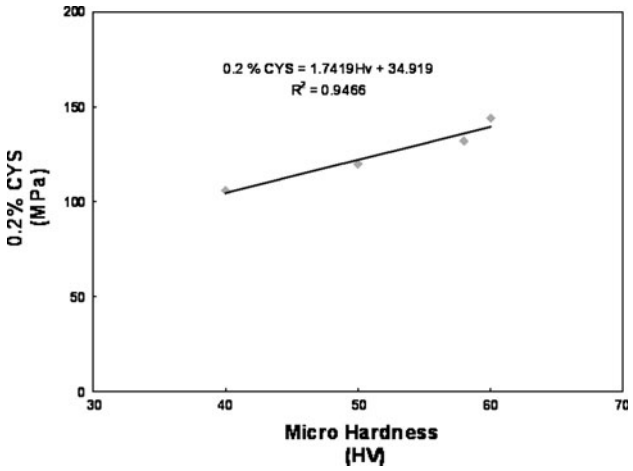

Fig. 5 Linear relationship between microhardness and 0.2% CYS of synthesized monolithic Mg and hybrid Mg/Al–CNT nano-composites

[7, 28, 32]. The increase in the compressive strength of Mg/Al–CNT nano-composites can be attributed to the following factors: (i) dislocation generation due to elastic modulus mismatch and coefficient of thermal expansion mismatch between the matrix and reinforcement [32–34], (ii) Orowan strengthening mechanism [32, 34, 35], (iii) load transfer from matrix to reinforcement [32–34], (iv) grain refinement caused by the presence of hybrid Al–CNT nano-particles, (v) effect of deformation twinning [26, 27, 36], and (vi) crystallographic texture based on (0 0 0 2) basal plane and (1 0 −1 2) pyramidal plane orientations [37].

Regarding factor (i), the mismatch of CTE and elastic modulus between the Mg matrix ($\alpha_{Mg} = 28.9 \times 10^{-6}\ K^{-1}$, $G_{Mg} = 17.3$ GPa [27]) and hybrid Al–CNT nano-particles ($\alpha_{Al-CNT} = 26.03–26.27 \times 10^{-6}\ K^{-1}$, $G_{Al-CNT} = 37.52–90.50$ GPa) leads to dislocation generation in the vicinity of the interface [20, 33]. A higher dislocation density in the nano-composite yields a higher level of internal stress [20]. The values for hybrid Al–CNT nano-particles vary since the content of Al also varies within different hybrid Al–CNT nano-particle formulations. Rule of mixtures was used for the calculation of CTE_{Al-CNT} and α_{Al-CNT}. To the best of the authors' knowledge, there is no reliable CTE and G data currently available for CNT. The CNT has a similar hexagonal arrangement of carbon atoms as the graphite crystal. Regarding CTE, the CTE of graphite crystal α_a of $21.5 \times 10^{-6}\ K^{-1}$ (0–150 °C) in the a-axis [38] (along the CNT length) was used. The shear modulus (G) was taken as 0.47 TPa [39] based on conducted simulations. The respective values for Al were taken as: $\alpha_{Al} = 26.49 \times 10^{-6}\ K^{-1}$ and $G_{Al} = 27$ GPa [7]. The geometrically necessary dislocation density due to elastic modulus [40] and CTE [41] mismatch are, respectively, given by:

$$\rho_{EM} = \frac{\gamma^m}{b\lambda} \tag{2}$$

$$\rho_{CTE} = \frac{10 f \varepsilon}{b(1-f)\bar{d}} \tag{3}$$

where γ^m is the shear strain in the matrix, λ is the local length scale of the deformation field which can be regarded as the distance whereby dislocations generated at the reinforcements are restrained from movement, b is the Burgers vector, f is the volume fraction of hybrid particles, ε is the misfit strain due to the different CTEs of Mg, and hybrid Al–CNT nano-particles, and $\bar{d}$ is the average diameter of hybrid nano-particles. The contribution of these geometrical dislocations in the enhanced strength of hybrid Mg/Al–CNT nano-composites can be obtained by the Taylor dislocation strengthening mechanism as follows:

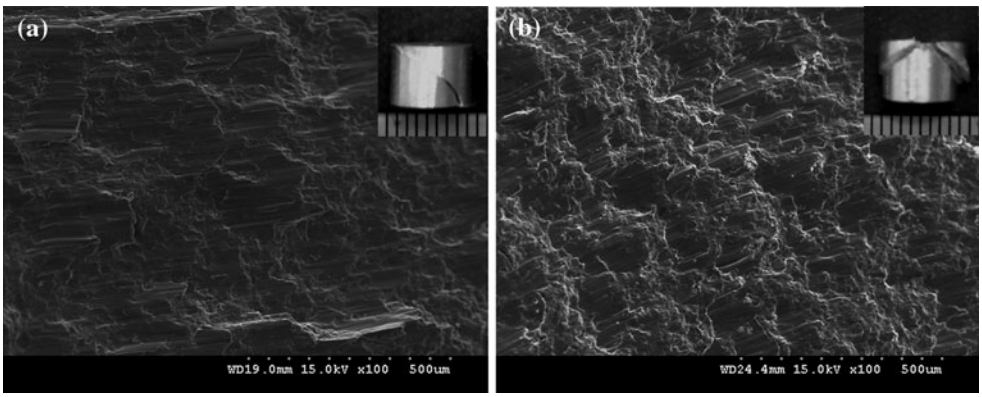

Fig. 6 Fractographs showing: **a** prominent shear bands in the case of monolithic Mg and **b** mixed mode of shear and brittle fracture in the case of Mg/Al–CNT nano-composites (*Insets*: fractured samples in compression)

$$\Delta\sigma_{\mathrm{EM}} = \sqrt{3}\alpha\mu_{\mathrm{m}}b\sqrt{\rho_{\mathrm{EM}}} \tag{4}$$

$$\Delta\sigma_{\mathrm{CTE}} = \sqrt{3}\beta\mu_{\mathrm{m}}b\sqrt{\rho_{\mathrm{CTE}}} \tag{5}$$

where $\Delta\sigma_{\mathrm{EM}}$ and $\Delta\sigma_{\mathrm{CTE}}$ are the stress increment due to elastic modulus and coefficient of thermal expansion mismatch between the matrix and hybrid Al–CNT nano-particles, respectively, α and β are the strengthening coefficient and μ_{m} is the shear modulus of the matrix.

Regarding factor (ii), the strength increase in the case of hybrid Mg/Al–CNT nano-composites can be also partly attributed to the interaction of hybrid Al–CNT nano-particles with dislocations. This interaction can be interpreted by use of the Orowan strengthening mechanism. In this mechanism a dislocation line loops around the hybrid Al–CNT nano-particles in the way of its advancement, provided the particle is sufficiently formed and has an atomically non-coherent interface with the matrix. These loops lead to high work hardening rates and help to strengthen the nano-composites. The contribution of Orowan strengthening mechanism to the enhanced yield strength of hybrid Mg/Al–CNT nano-composites can be expressed as below:

$$\Delta\sigma_{\mathrm{Orawan}} = M\frac{0.4\mu_{\mathrm{m}}b}{\Pi\bar{\lambda}}\frac{\ln\left(\frac{\bar{d}}{b}\right)}{\sqrt{1-\upsilon_{\mathrm{Mg}}}} \tag{6}$$

where M is a strengthening coefficient, $\bar{\lambda}$ is the mean inter-particles distance given by $\bar{\lambda} = \bar{d}\left(\sqrt{\frac{\Pi}{4f}} - 1\right)$, and υ_{Mg} is the Poisson's ratio for Mg.

Regarding factor (iii), effective load transfer from matrix to reinforcement can be regarded as another strengthening mechanism which can be responsible for the increased strength in the case of hybrid Mg/Al–CNT nano-composites. This strengthening mechanism strongly depends on interfacial bonding between the hybrid Al–CNT nano-particles and Mg matrix as well as volume fraction of hybrid nano-particles. The contribution of this strengthening mechanism can be expressed as below:

$$\sigma_{\mathrm{c}} = \sigma_{\mathrm{m}}\left(1 + \frac{(L+t)A}{4L}\right)f + \sigma_{\mathrm{m}}(1-f) \tag{7}$$

where σ_{c} and σ_{m} are the yield stress of nano-composite and monolithic Mg, respectively, L is the size of particles parallel to the load direction, and t is the thickness of particles. For the equiaxed particles, an increment in the yield stress due to load transfer $\Delta\sigma_{\mathrm{LT}}$ can be expressed by [42]:

$$\Delta\sigma_{LT} = \sigma_c - \sigma_m = 0.5f\sigma_m \tag{8}$$

Regarding factor (iv), grain size strengthening mechanism is another strengthening mechanism which is mainly responsible for the increased strength of nano-composites compared to monolithic Mg. The strengthening of nano-composites from grain size reduction fundamentally comes from the mutual disturbance of slip among the grains. Here, the motion of dislocation across the grain boundary is impeded and the yield stress can be estimated by the Hall–Petch equation as below:

$$\sigma_y = \sigma_0 + K_y d_{\mathrm{Mg}}^{-0.5} \tag{9}$$

where σ_0 is a constant stress of uncertain origin (back-stress); K_{y} is the Hall–Petch coefficient, and d_{Mg} is the average Mg grain size.

Regarding factor (v), twinning can also be responsible for the enhanced strength of hybrid Mg/Al–CNT nano-composites. In the case of twinning, twinning produces additional barriers to dislocations movement which is similar to reducing grain size [26, 27, 43]. Twin boundaries act as grain boundaries and reduce the slip path in the untwinned region leading to increase in strength. The following schematic (Fig. 7) and equation illustrates this:

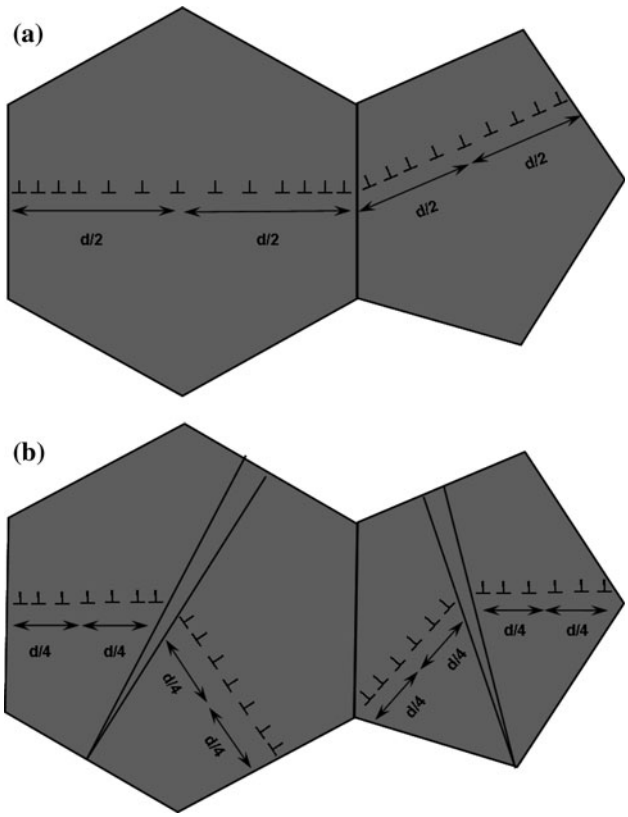

Fig. 7 Schematic representation of accumulation of dislocations in the case of **a** untwinned grains and **b** twinned grains

$$\text{Untwinned}: \sigma_{y_1} = \sigma_0 + K_y d^{-0.5} \quad \text{for } (d) \tag{10}$$

$$\text{Twinned}: \sigma_{y_2} = X_1\sigma_0 + K_y\left(\frac{d}{2}\right)^{-0.5} \quad \text{for } \left(\frac{d}{2}\right),\ X_1 > 1$$

$$\sigma_{y_2} = X_1\sigma_0 + X_2K_y(d)^{-0.5} \quad X_2 = \left(\frac{1}{2}\right)^{-0.5} > 1$$

$$\Rightarrow \sigma_{y_2} > \sigma_{y_1} \tag{11}$$

The formation of twin boundaries reduce the slip path of dislocations and may contribute to strengthening of materials based on Eq. 11.

Regarding factor (vi), crystallographic texture based on basal (0 0 0 2) plane and (1 0 −1 2) pyramidal plane orientations may contribute to strengthening in hybrid Mg–Al–CNT nano-composites. Considering the limited slip system activation in the HCP unit cell based structure of the Mg matrix at room temperature, it was noted that the enhancement in compressive strength occurred partly due to the crystallographic texture difference between the nano-composite matrix and monolithic material. In comparison of crystallographic texture, Mg–Al–CNT nano-composites exhibited (1 0 −1 0) and (0 0 0 2) dominant textures in the transverse and longitudinal directions, respectively, as listed in Table 3 and shown in Fig. 3, unlike monolithic Mg. For these (1 0 −1 0) and (0 0 0 2) dominant textures, basal slip is made most difficult due to low resolved shear stress (RSS) for slip based on the zero angle between the (0 0 0 2) basal plane and the vertical axis as shown in Fig. 3. Regarding twinning, pyramidal (1 0 −1 2) plane is the desired plane for the tension twinning in Mg. Considering the X-ray diffraction from crystallographic planes parallel or near-parallel (±20°) [21–23] to the plane containing the direction vector, the reorientation of pyramidal planes in hybrid Mg–Al–CNT nano-composites compared to monolithic Mg makes the occurrence of tension twinning during compression testing more difficult (see Fig. 3). In terms of crystallographic texture, complications in basal slip and twinning may be responsible for the observed enhancement in compressive strength of hybrid nano-composites compared to monolithic Mg. In compressed monolithic Mg, activation of basal slip with strong basal texture after twinning saturation and slip-twin interaction (see Fig. 2b) leads to fast work hardening increment. Similarly, the net effect of crystallographic change in Mg–Al–CNT nano-composites due to addition of hybrid Al–CNT nano-particles can be taken as contribution to strengthening. This is assuming tension twinning and then basal and finally non-basal slips (in that order) are responsible for the deformation during compression, as mentioned earlier in the introduction. The significant reduction in failure strain in the case of hybrid Mg/Al–CNT nano-composites compared to monolithic Mg is attributed partially to these texture effects also.

The contribution of the various strengthening mechanisms (factor (i)–(vi)) and the consequent synergetic combination of both hybrid Al–CNT nano-particles and monolithic Mg account for the improvement in strength of hybrid Mg/Al–CNT nano-composites compared to monolithic Mg.

The work of fracture of hybrid Mg/Al–CNT nano-composites was larger than that of monolithic Mg and was improved by +36% in the case of Mg/1.50Al–0.18CNT nano-composite (see Table 3). This can be mainly attributed to the enhanced compressive strength since failure strain was compromised compared to monolithic Mg. Work of fracture expresses the ability of the material to absorb energy up to fracture and corresponds to the area under the engineering stress–strain curve up to the point of fracture [33, 34]. The results thus clearly reveal the enhanced damage tolerance capability of monolithic Mg when reinforced with hybrid Al–CNT particles in nano-length scale.

Fracture behavior

Macroscopically, all monolithic Mg samples failed via one principle crack which was inclined at 45° to the

compressive axis (see Fig. 6a) while all the hybrid Mg–Al–CNT nano-composites shattered into three parts with cracks also inclined at 45° to the compression axis (see Fig. 6b). Examination of fracture surfaces of monolithic Mg revealed smooth shear bands which can be attributed to twinning shear. However, fracture surface of the nano-composites were rough and showed mixed mode of shear and brittle fracture [44].

Conclusions

The following conclusions can be made from the experimental findings of this study.

Conventional solid state powder metallurgy technique using rapid microwave sintering and hot extrusion can be successfully used to synthesize near dense Mg nano-composites containing hybrid Al–CNT nano-particles.

Hybrid Mg microstructures synthesized in the present study exhibited reasonably uniform distribution of hybrid Al–CNT nano-particles up to Al content of 1.00 wt%.

The presence of hybrid Al–CNT nano-particles refines the Mg grain size significantly and stabilizes the grains by providing pinning sites against grain growth.

The compressive strength of all hybrid Mg/Al–CNT nano-composites is significantly higher compared to monolithic Mg. This strength enhancement can be attributed to (a) dislocation generation due to elastic modulus mismatch and coefficient of thermal expansion mismatch between the matrix and hybrid Al–CNT nano-particles, (b) Orowan strengthening mechanism, (c) reduction in average matrix grain size, and (d) presence of twinning.

Considering of work of fracture, hybrid Mg/Al–CNT nano-composites showed significant improvement which mostly can be attributed to the strength enhancement since failure strain was compromised compared to monolithic Mg.

Acknowledgements The authors gratefully acknowledge the financial support from Qatar National Research Foundation through research grant # NPRP08-424-2-171 (R-265-000-346-597) and NUS research scholarship for supporting the research effort.

References

1. Clyne TW, Withers PJ (1993) An introduction to metal matrix composites. Cambridge University Press, Cambridge
2. Goh CS, Gupta M, Wei J, Lee LC (2007) J Compos Mater 41:2325
3. Goh CS, Wei J, Gupta M (2007) Proceedings of the materials division 433
4. Hassan SF, Gupta M (2007) J Compos Mater 41:2533
5. Thakur SK, Kwee GT, Gupta M (2007) J Mater Sci 42:10040. doi:10.1007/s10853-007-2004-0
6. Nguyen QB, Gupta M (2008) Compos Sci Technol 68:2185
7. Habibi MK, Joshi SP, Gupta M (2010) Acta Mater. doi:10.1016/j.actamat.2010.07.028
8. Wong EW, Sheehan PE, Lieber CM (1997) Science 277:1971
9. Yao Z, Zhu CC, Cheng M, Liu J (2001) Comput Mater Sci 22:180
10. Paramsothy M, Hassan SF, Srikanth N, Gupta M (2010) J Nanosci Nanotechnol 10:956
11. Li Q, Viereckl A, Rottmair CA, Singer RF (2009) Compos Sci Technol 69:1193
12. George R, Kashyap KT, Rahul R, Yamdagni S (2005) Scr Mater 53:1159
13. Jiang L, Jonas JJ, Luo AA, Sachdev AK, Godet S (2007) Mater Sci Eng A 445–446:302
14. Brown DW, Agnew SR, Bourke MAM, Holden TM, Vogel SC, Tomé CN (2005) Mater Sci Eng A 399:1
15. Staroselsky A, Anand L (2003) Int J Plast 19:1843
16. Meyers MA, Vöhringer O, Lubarda VA (2001) Acta Mater 49:4025
17. Koike J, Kobayashi T, Mukai T et al (2003) Acta Mater 51:2055
18. Chang LL, Wang YN, Zhao X, Qi M (2009) Mater Charact 60:991
19. Yoo MH (1981) Metall Trans A 12:409
20. Goh CS, Wei J, Lee LC, Gupta M (2006) Nanotechnology 17:7
21. Habibi MK, Paramsothy M, Hamouda AMS, Gupta M (2010) Compos Sci Technol (in press)
22. Goh CS, Wei J, Lee LC, Gupta M (2008) Compos Sci Technol 68:1432
23. Paramsothy M, Hassan SF, Srikanth N, Gupta M (2008) J Phy D 41
24. Paramsothy M, Gupta M, Srikanth N (2008) J Compos Mater 42:1297
25. Barnett MR (2007) Mater Sci Eng A 464:1
26. Salem AA, Kalidindi SR, Doherty RD (2003) Acta Mater 51:4225
27. Salem AA, Kalidindi SR, Semiatin SL (2005) Acta Mater 53:3495
28. Han BQ, Dunand DC (2000) Mater Sci Eng A 277:297
29. Zhong XL, Wong WLE, Gupta M (2007) Acta Mater 55:6338
30. Gupta M, Lai MO, Soo CY (1996) Mater Sci Eng A 210:114
31. Courtney TH (2000) Mechanical behavior of materials. McGraw-Hill, Michigan
32. Száraz Z, Trojanová Z, Cabbibo M, Evangelista E (2007) Mater Sci Eng A 462:225
33. Hassan SF, Gupta M (2006) J Mater Sci 41:2229. doi:10.1007/s10853-006-7178-3
34. Wong WLE, Gupta M (2007) Compos Sci Technol 67:1541
35. Dai LH, Ling Z, Bai YL (2001) Compos Sci Technol 61:1057
36. Barnett MR, Keshavarz Z, Beer AG, Atwell D (2004) Acta Mater 52:5093
37. Hall D, Bacon DJ (2002) Introduction to dislocation. Oxford Butterworth-Heinemann, Oxford
38. Kelly BT (1981) Physics of graphite. Applied Science Publishers, London
39. To CWS (2006) Finite Elem Anal Des 42:404
40. Kouzeli M, Mortensen A (2002) Acta Mater 50:39
41. Arsenault RJ, Shi N (1986) Mater Sci Eng 81:175
42. Aikin RM Jr, Christodoulou L (1991) Scr Metall Mater 25:9
43. Karaman I, Sehitoglu H, Beaudoev AJ, Chumlyakov YI, Maier HJ, Tomé CN (2000) Acta Mater 48:2031
44. Barnett MR (2007) Mater Sci Eng A 464:8